Transport and diffusion in the embedding map

N. Nirmal Thyagu* and Neelima Gupte†
Department of Physics, Indian Institute of Technology Madras, Chennai 600036, India
(Received 22 December 2008; revised manuscript received 20 April 2009; published 5 June 2009)

We study the transport properties of passive inertial particles in two-dimensional (2D) incompressible flows. Here, the particle dynamics is represented by the four-dimensional dissipative embedding map of the 2D area-preserving standard map which models the incompressible flow. The system is a model for impurity dynamics in a fluid and is characterized by two parameters, the inertia parameter α and the dissipation parameter γ. The aerosol regime, where the particles are denser than the fluid, and the bubble regime, where they are less dense than the fluid, correspond to the parameter regimes $\alpha>1$ and $\alpha<1$, respectively. Earlier studies of this system show a rich phase diagram with dynamical regimes corresponding to periodic orbits, chaotic structures, and mixed regimes. We obtain the statistical characterizers of transport for this system in these dynamical regimes. These are the recurrence time statistics, the diffusion exponent, and the distribution of jump lengths. The recurrence time distribution shows a power-law tail in the dynamical regimes, where there is preferential concentration of particles in sticky regions of the phase space, and an exponential decay in mixing regimes. The diffusion exponent shows behavior of three types—normal, subdiffusive, and superdiffusive, depending on the parameter regimes. Phase diagrams of the system are constructed to differentiate different types of diffusion behavior, as well as the behavior of the absolute drift. We correlate the dynamical regimes seen for the system at different parameter values with the transport properties observed at these regimes and in the behavior of the transients. This system also shows the existence of a crisis and unstable dimension variability at certain parameter values. The signature of the unstable dimension variability is seen in the statistical characterizers of transport. We discuss the implications of our results for realistic systems.

DOI: 10.1103/PhysRevE.79.066203 PACS number(s): 05.45.−a

I. INTRODUCTION

The study of transport properties of impurities in fluid flows is a problem of important practical interest. These properties can have serious implications for pollution in the atmosphere, plankton populations in the ocean, and diverse engineering applications. There is evidence that transport processes occurring in nature, e.g., the atmosphere [1], are quasi-two-dimensional (quasi-2D) [2,3]. The chaotic advection [4,5] of impurities which are modeled by inertial particles of finite size in flows of different types has been studied both in the case of passive particles [6–8] and in the case of active particles that can react with the surroundings [9,10]. Impurity dynamics in such two-dimensional fluid flows can be effectively modeled by the bailout embedding maps of 2D area-preserving maps [11,12]. We attempt to understand the dynamical and statistical properties of impurity transport in 2D incompressible flows by studying such embedding maps.

The Lagrangian dynamics of small spherical tracers in two-dimensional incompressible fluid flows is described by the Maxey-Riley equations. These are further simplified under various approximations to give a set of minimal equations called the embedding equations where the fluid flow dynamics is embedded in a larger set of equations which includes the difference between the particle and fluid velocities [11–19]. Although the Lagrangian dynamics of the underlying fluid flow is incompressible, the particle motion is compressible [14] and has regions of contraction and expansion. The density grows in the former giving rise to clusters and falls in the latter giving rise to voids. The properties of the base flow have important consequences for the transport and mixing of particles. Map analogs of the embedding equations have also been constructed for cases where the fluid dynamics is modeled by area-preserving maps which essentially retain the qualitative features of the flow [15]. The embedded dynamics in both cases is dissipative in nature. Here, we study the embedded standard map.

We study several statistical characterizers of transport properties in different dynamical regimes of the system. These are the recurrence time statistics, diffusion and drift quantifiers, and the distribution of jump lengths. The first of these, viz., the recurrence time statistics, show signatures of the dynamical regime of the system. The cumulative probability distribution of the recurrence times (sometimes called the complementary cumulative distribution [16]), in the regime where chaotic structures are seen, shows the power-law tail characteristic of dynamics in an inhomogeneous phase space with sticky regions. In contrast, in the regimes where full mixing is seen, the recurrence time distribution (RTD) shows exponential decay characteristic of rapid mixing. Earlier studies of the connection between the recurrence time statistics and the transport of particles had established that normal transport occurs for cases where the recurrence time distribution shows exponential behavior, while anomalous transport occurs if there is a power-law recurrence time distribution [20,21]. In the embedding map studied here, we observe that there is a crossover from exponential behavior to power-law behavior in the recurrence time distribution in different dynamical regimes implying that there are some dynamical regimes which are characterized by anomalous transport. The diffusion properties corresponding to these

*nirmal@physics.iitm.ac.in
†gupte@physics.iitm.ac.in

cases are further explored. We also comment on the differences between the behavior of aerosols and that of bubbles.

The diffusion studies show that the system can show a variety of regimes corresponding to generalized diffusive behavior. Three types of diffusion, viz., normal or Brownian diffusion, superdiffusion, and subdiffusive behavior, are identified. A phase diagram is constructed to classify and demarcate the regions of diffusion in the α-γ parameter space. Apart from the usually observed normal and superdiffiusive cases, the embedding map has two subclasses of subdiffusion—one associated with trapping with stationary states and the other with trapping with nonstationary states. The regions where ballistic diffusion is observed in the phase space are identified in the α-γ phase diagram. Similarly, the areas where the average drift is zero are also likewise identified in the phase diagram. The diffusive behavior of the system is compared with the dynamical regimes. Our inferences can have implication for the transport of pollutants in the atmosphere or other real application contexts.

The signature of the different dynamical regimes can also be seen in the transient behavior of the system. The jump length distributions, where the jump length is defined as the Euclidean distance between successive iterates, have envelopes which can be fitted by a heavy tailed Levy distribution in the chaotic structure regime, which are characterized by sticky regions in the inhomogeneous phase space, and by a Gaussian envelope in the mixing regimes. The cumulated jump length distributions here show power-law behavior for the sticky regimes and cumulated Gaussians for the mixing regimes.

In the aerosol regime of the embedding map, the plot of the largest Lyapunov exponent shows signatures of unstable dimension variability (UDV) at certain parameter values. The recurrence time statistics shows the signature of the UDV, as does the diffusion exponent. We discuss the consequences of this UDV for the transport properties of the system. We summarize the implications of our results.

II. DYNAMICAL REGIMES AND PHASE DIAGRAM

The dynamics of inertial particles in a flow has been shown to be modeled by the bailout embedding equation [11],

$$\frac{d\mathbf{v}}{dt} - \alpha\frac{d\mathbf{u}}{dt} = -\gamma(\mathbf{v}-\mathbf{u}). \tag{1}$$

Here, the velocity of the particle is $\mathbf{v}=d\mathbf{x}/dt$ and the velocity field of the fluid flow is $\mathbf{u}(x,y,t)$ for a 2D fluid. The inertial parameter α is related to the particle and fluid densities, ρ_p and ρ_f, by the equation $\alpha=3\rho_f/(\rho_f+2\rho_p)$. Thus, the $\alpha<1$ regime corresponds to the aerosols, and the $\alpha>1$ regime corresponds to the bubbles. The dissipation parameter γ is defined by $\gamma=2\alpha/3\mathrm{St}$, where St is the Stokes number, and provides a measure of the contraction or expansion in the phase space of the particle. The particle dynamics is dissipative in nature. A map analog of Eq. (1) has been constructed [11,13]. This has the form

$$\mathbf{x}_{n+1} = \mathbf{M}(\mathbf{x}_n) + \boldsymbol{\delta}_n,$$

$$\boldsymbol{\delta}_{n+1} = e^{-\gamma}[\alpha\mathbf{x}_{n+1} - \mathbf{M}(\mathbf{x}_n)]. \tag{2}$$

Here, the area-preserving map $\mathbf{M}(\mathbf{x})$ represents the incompressible fluid acting as the base flow. The vector $\mathbf{x}$ represents the position of the particle and the vector $\boldsymbol{\delta}$ defines the detachment of the particle from the fluid velocities [11]. In our study, the dynamics of the base fluid flow has been represented by the 2D standard map, as it is a prototypical area-preserving system [22], and is widely used as a test bed in a variety of transport problems [23]. The evolution equations of the standard map are

$$x_{n+1} = x_n + \frac{K}{2\pi}\sin(2\pi y_n),$$

$$y_{n+1} = y_n + x_{n+1}, \tag{3}$$

with periodic boundary conditions such that $x,y\in[-1,1]$. We fix the parameter $K=2$ in our study. The phase space of the standard map contains both regular and chaotic regions for this value. Substituting the form of the standard map as $\mathbf{M}$ in the embedding map equation above, we get a four-dimensional (4D) embedding map,

$$x_{n+1} = x_n + \frac{K}{2\pi}\sin(2\pi y_n) + \delta_n^x,$$

$$y_{n+1} = x_n + y_n + \frac{K}{2\pi}\sin(2\pi y_n) + \delta_n^y,$$

$$\delta_{n+1}^x = e^{-\gamma}[\alpha x_{n+1} - (x_{n+1} - \delta_n^x)],$$

$$\delta_{n+1}^y = e^{-\gamma}[\alpha y_{n+1} - (y_{n+1} - \delta_n^y)]. \tag{4}$$

This map is invertible and dissipative. We study the behavior of the map in the parameter regimes $0<\alpha<3$ and $0<\gamma<1$. Thus, our study encompasses both the aerosol regime, i.e., $\alpha<1$, and the bubble regime, $\alpha>1$. The dynamical regimes of the system have been cataloged in the phase diagram in Ref. [12] for the same range of parameters. A variety of dynamical behaviors can be seen at different values of α and γ. These include periodic behavior, chaotic structures [Fig. 3(a)], and fully mixing regimes Fig. 5(a). A detailed phase diagram of the system can be found in Fig. 1 (see Ref. [12] for a detailed description of the method of construction of the phase diagram) [24].

Since the map represents the Lagrangian dynamics of particles, the chaotic structures seen due to the stickiness of the phase space correspond to the preferential concentration of particles. On the other hand, a uniform distribution of particles can be seen in the well mixed regimes of phase space. Thus, the phase diagram of the system has important implications for the transport properties of the system. In Sec. III, we examine these transport properties via statistical characterizers. We start with the recurrence time statistics.

III. RECURRENCE TIME STATISTICS

The statistics of recurrence times are of fundamental importance in the study of chaotic systems [25–27]. These in-

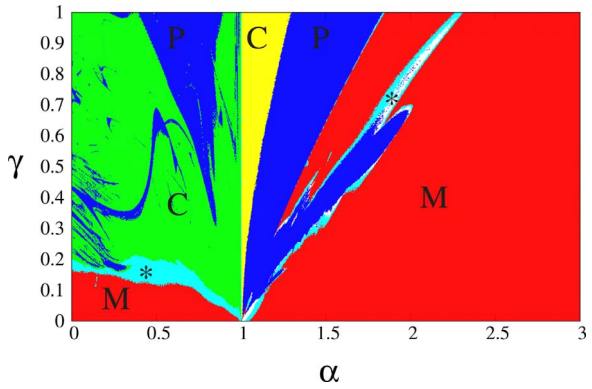

FIG. 1. (Color online) The phase diagram showing the three dynamical regimes in the embedding map in the α-γ parameter space. The regions marked by red ("M") show mixing and the regions marked by blue ("P") have periodic orbits. Chaotic structures are seen in the regions marked by green and yellow ("C") in the aerosol and bubble regions, respectively. There are some regions marked by light blue (labeled by "*") which have chaotic structure over a mixing background in phase space.

volve the study of recurrences of a given dynamical state of the system in finite time. The first recurrence time of a trajectory of a system can be defined to be the time τ_1 taken for a trajectory, which starts from a small subset ξ of the phase space of the system to return to the same subset ξ in the limit where the volume of the subset $\xi \to 0$ (see Fig. 2). The trajectory may return to the subset at subsequent times $\tau_2, \tau_3, \ldots, \tau_n$, with τ_n being called the nth recurrence time. A set of the time intervals τ_i can be obtained in the long time limit to give the recurrence time distribution of that trajectory. The average recurrence time of the subset ξ is calculated by averaging over the recurrence times of the trajectories starting in the subset ξ, and the average recurrence time of the entire phase space can be obtained by averaging over the recurrence times of all the partitions in the phase space (see Refs. [21,28] for more rigorous definitions).

Extensive studies of the mean recurrence times have been carried out in the case of chaotic Hamiltonian systems [29]. Generally, Hamiltonian systems are not fully hyperbolic, and the phase space of such Hamiltonian, as well as that of area-preserving systems, contains regular islands and chaotic mixing regions in the phase space. A trajectory that originates in the chaotic region can stick to the neighborhood of the regular islands intermittently and, as a result, influence long time properties such as the recurrence times giving rise to power-law decays in the recurrence time distribution [30]. The cumulative recurrence time distribution shows exponential decay for uniformly hyperbolic system, where mixing is strong. In contrast, power-law decay is observed for the recurrence time distributions of systems that have inhomogeneous phase space [16].

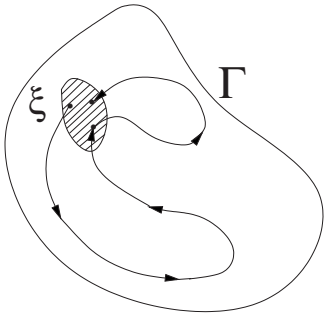

FIG. 2. The schematic illustration of the recurrence phenomena in an invariant set Γ. A trajectory starting in a small partition ξ is revisiting the partition in finite time. Here only the first and the second recurrences are shown.

In the case of area-preserving maps, such as the standard map, the Poincaré recurrence time statistics shows two limiting cases. First, for the chaotic strong coupling limit (high values of the nonlinearity parameter K), where mixing is prominent in the phase space, the recurrence time distributions show exponential decay as functions of time. Second, for the near integrable weak coupling limit (small values of K, $K < K_{critical} = 0.971\,635\,406\,31$), the distributions show inverse power-law behavior [31]. At $K = K_{critical}$ the distribution shows a power-law decay [29].

The base flow of our embedding map is the area-preserving standard map, with the recurrence time statistics described above. However, the dynamics of the inertial particles, as described by the embedding map, is dissipative in nature. It is therefore interesting to study the recurrence time statistics of the embedding map, see how the statistics of the inertial particles differs from the statistics of the base flow, and also see the effects of different dynamical regimes. We do this in the current section.

We study the recurrence time statistics in the two-dimensional phase space spanned by the configuration space coordinates x-y and compare this with the recurrence time statistics in the four-dimensional phase space $(x, y, \delta_x, \delta_y)$. For the 2D statistics, the two-dimensional configuration space x, y with $x \in [-1, 1]$ and $y \in [-1, 1]$ is divided into a grid of 50×50 boxes and 200 uniform random initial conditions are evolved for 1×10^6 time steps, with 5000 iterations as transients. Each trajectory is associated with the box it visits immediately after the transients. The average recurrence time associated with any box is the recurrence time averaged over the initial conditions that are associated with that box [32]. We compare the general features of the recurrence time distributions for the two aperiodic dynamical regimes, viz., the chaotic structure regime and the mixing regime (see Fig. 1).

First, let us consider the chaotic structure regime with the parameters $\alpha = 0.4$ and $\gamma = 0.4$. We first discuss the 2D recurrences. It is clear from the x-y phase space plot of Fig. 3(a) that the phase space in the chaotic structure regime is inhomogeneous. If the region available to all the trajectories for motion is called Γ, there are some special regions S contained in Γ where the trajectory visits more often than others. Hence, in the phase space plots, the region S is darker than the background Γ [see Fig. 3(a)]. These darker regions are identified as the sticky regions and have an important effect on the recurrence time statistics. The invariant density ρ supported by the x-y space is plotted in Fig. 3(b). To obtain the invariant density, random initial conditions were uniformly spread in the phase space covered by a grid, and the total number of times that trajectories visit a particular box in its

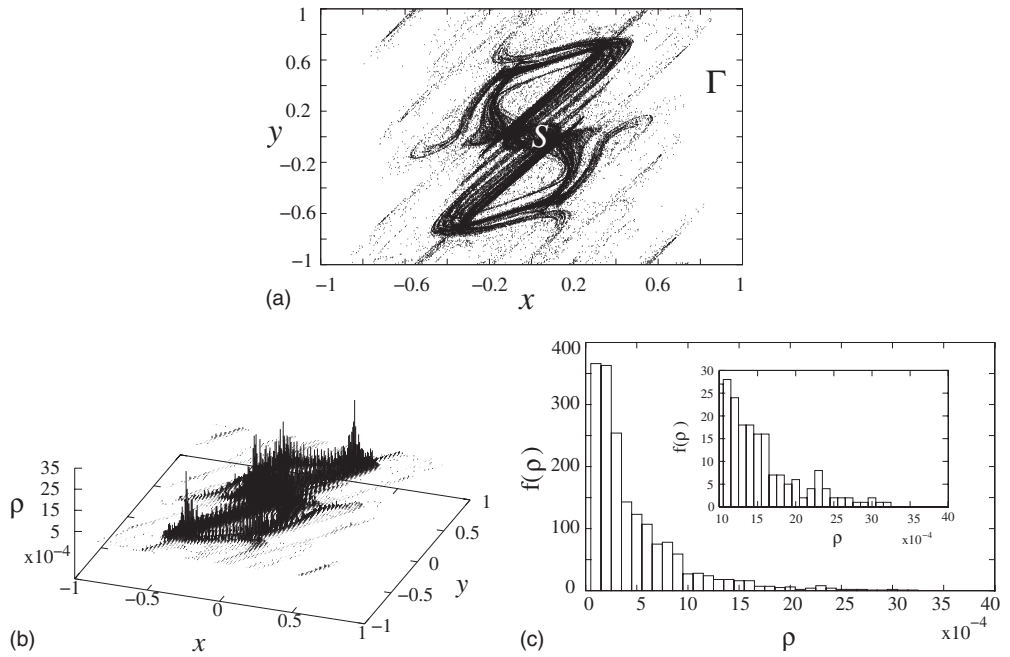

FIG. 3. (a) The phase space plot with chaotic structures (α=0.4 and γ=0.4). The darker regions are visited more often and the recurrence times in these areas are longer. (b) The three-dimensional invariant density plot of the attractor in the x-y plane shows larger values of the invariant density ρ where the region is sticky. (c) The histogram is plotted to show the distribution of the normalized invariant density ρ.

itinerary was counted [33]. It is clear that the value of the invariant density in the sticky regions is much higher than that in the background. The histogram of the normalized invariant density is plotted in Fig. 3(c) and clearly shows that the major part of the phase space (the background) supports very small values of the invariant density and the large values of the invariant density are concentrated on a small subset of the phase space, the sticky regions, or the regions where the chaotic structure is seen [34]. Such sticky regions have also been found in area-preserving maps and experiments in fluids [6,35].

The cumulative recurrence time statistics in the chaotic structure case show a power-law decay for large times [see Fig. 4(a)],

$$P(\tau) \sim \tau^{\zeta'}. \tag{5}$$

Here, the exponent of the cumulative probability distribution ζ' and the exponent ζ of the probability distribution are related by $\zeta=\zeta'-1$, as both the distributions show power-law behavior at large times. In contrast, at short times, the cumulative RTD shows an exponential decay [see Fig. 4(b)],

$$P(\tau) \sim e^{b\tau}. \tag{6}$$

We compare the 2D recurrences seen here with the 4D recurrences in the full x-y, δ_x-δ_y space. The four-dimensional recurrence time distribution corresponding to the chaotic structure case is plotted along with the two-dimensional recurrence time distribution in Figs. 4(a) and 4(b). Since the 2D space is a projection of the 4D space on the x-y plane, recurrences to the 4D space are expected to be longer than the recurrences to the 2D space; hence the distribution in four dimensions has shifted to higher τ values. The character of the graph is unaltered, namely, it shows a power-law decay though the exponent is $\zeta_{4D}=-2.6$, while the 2D exponent is $\zeta_{2D}=-2.9$. In the short time limit, the distribution is exponential for both cases and the constant b takes the values

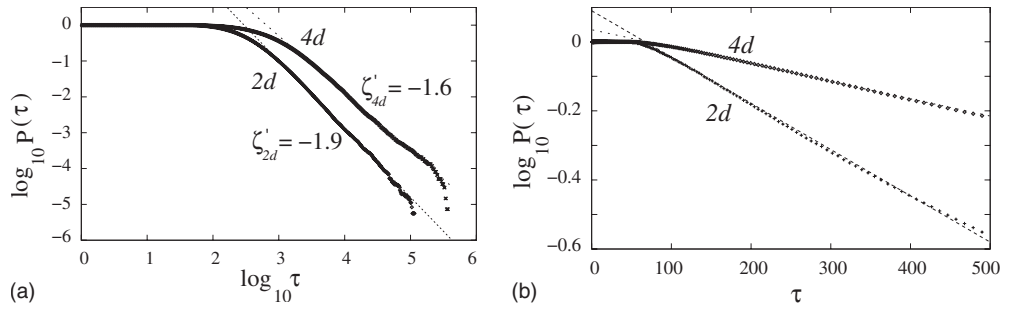

FIG. 4. (a) The complementary cumulative distribution of recurrence times at this parameter value shows a power-law decay in the long time limit, with the exponent $\zeta_{2D}=\zeta'_{2D}-1=-2.9$ for the 2D recurrence and $\zeta_{4D}=\zeta'_{4D}-1=-2.6$ for the 4D recurrence. (b) The log-linear plot in the short time limit shows an exponential decay, with the slope=−0.001 34 for the 2D case and slope=−0.0005 for the 4D case.

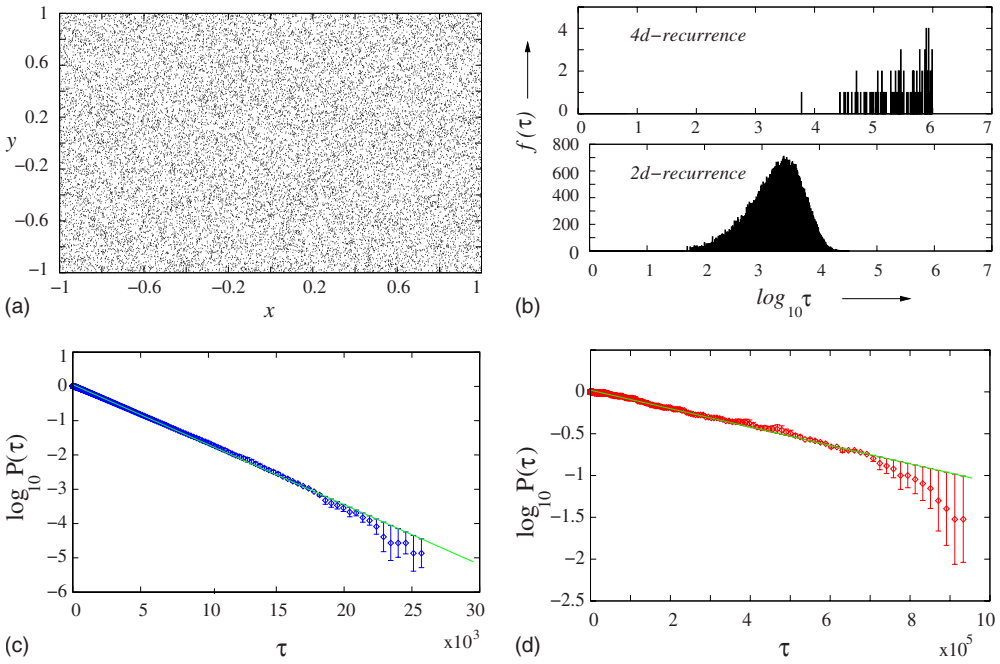

FIG. 5. (Color online) (a) The phase space plot in a mixing regime (α=2.8 and γ=0.4). We can see that there is no preferential concentration of particles in any region of the phase space. (b) The histograms of the distribution of recurrence times in the four-dimensional case (top) and the two-dimensional case (bottom). The log-linear plots of the complementary cumulative distribution of recurrence times in (c) two dimensions with slope of −0.000 175 and (d) four dimensions with slope of −0.000 001 1.

b_{2D}=−0.001 34 and b_{4D}=−0.0005 for the two-dimensional and the four-dimensional recurrences, respectively. We note that the values of ζ and b are not universal and change with the parameter values of α and γ. However, the qualitative behavior of the recurrence time distribution remains the same at other parameter values in the chaotic structure regime [36].

In the case of the area-preserving maps, the power-law scaling indicates that the phase space is inhomogeneous. In the case of the dissipative map discussed here, a similar effect is seen due to the existence of the chaotic structure or sticky regions in the phase space. The examination of the residence times of trajectories starting from arbitrary initial conditions shows that the trajectories spend 80% of their time in the sticky regions regardless of the initial conditions. Trajectories which start in the nonsticky regions of the phase space wander into the sticky regions and spend a long time there before emerging outside. This leads to long recurrence times. Other trajectories have short recurrence times. The exponential decay seen in the early part of the RTD corresponds to the short recurrences. On the other hand, the power-law scaling regime is due to the recurrences to the nonsticky regions. This accounts for the crossover from exponential to power-law behavior seen in the recurrence time distribution. Thus, the chaotic structures play the same role in the phase space for the embedding map as the islands seen in the area-preserving maps. However, there is no hierarchy in the chaotic structures unlike that in the case of the hierarchical islands of the area-preserving maps.

The behavior of the recurrence time distribution in the mixing regimes of the phase diagram is quite different. Here, unlike the chaotic structure case, the mixing is very strong and there are no preferential regions in the phase space which the particles visit more frequently or stick to for longer times. The phase space plot of a typical mixing regime can be seen in Fig. 5(a). The recurrence time distributions show exponential decay both in the 2D and the 4D cases, as is expected for the strongly mixing case. In Figs. 5(c) and 5(d) the log-linear plots of the RTD show the exponential decays with the slopes for the two-dimensional and four-dimensional cases to be −0.000 175 and −0.000 001 1, respectively. The histograms of the recurrence times for the two-dimensional and the four-dimensional cases are shown in Fig. 5(b). It is clear that the four-dimensional recurrence times are longer than the two-dimensional recurrence times. Also it is evident that the frequency of occurrence of the 4D recurrences is much smaller than the frequency of occurrence of the 2D recurrences [compare the values of $f(\tau)$ in both the ordinates of Fig. 5(b)].

In the chaotic structure case we saw a crossover from the exponential decay behavior at short times to power-law behavior at asymptotic times. This crossover behavior seen in the recurrence statistics signals a transition in the transport properties of the system [20]. We examine the transport properties using detailed diffusion studies and correlate them with the recurrence times and the dynamical regimes.

IV. DIFFUSION

The transport of passive inertial particles in flows can be described statistically by examining the dispersion as a function of parameters α and γ. We consider an ensemble of N initial particles distributed uniformly randomly in the phase space and evolve them in time. As the initial conditions

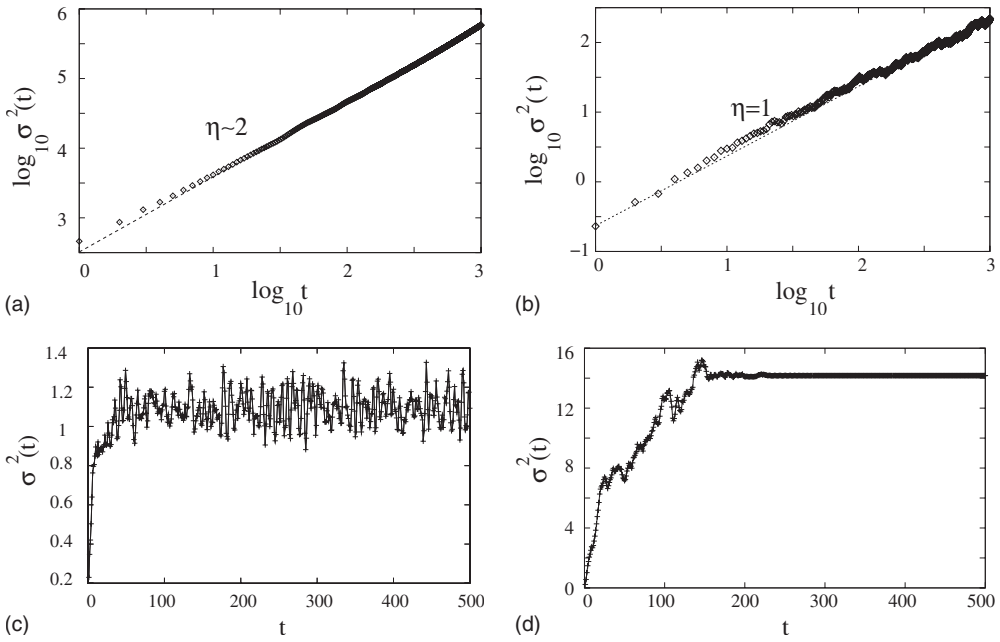

FIG. 6. The plot showing the variance of the particle cloud as it evolves in time. (a) Superdiffusive behavior is observed for parameters $\alpha=1.2$ and $\gamma=0.2$ with exponent $\eta=2.0135$. (b) Normal diffusion is seen for the parameters $\alpha=2.8$ and $\gamma=0.1$ with the exponent $\eta=1.006\ 11$ (error bars). Trapping regimes show the plateauing of the variance (c) with nonstationary states ($\alpha=0.5$ and $\gamma=0.5$) and (d) trapping with stationary states ($\alpha=1.5$ and $\gamma=0.8$).

evolve in time, the particle cloud drifts in the two-dimensional configurational space from the initial position, as well as the individual particles disperse from the moving cloud. The dispersion of particles is given by the variance of the displacement of particles σ^2,

$$\sigma^2(t) = \langle (\mathbf{x}(t) - \langle \mathbf{x}(t) \rangle)^2 \rangle \sim Dt^{\eta}. \tag{7}$$

Here $\mathbf{x}(t)$ is the position of a particle and $\langle \mathbf{x}(t) \rangle$ is the average position of all the particles at time t, both in the configuration space. The diffusion coefficient D and the exponent η quantify the type of diffusion. The angular brackets indicate the average over the ensemble. The configuration space in two dimensions considered here is the cover space, i.e., without the periodic boundary condition that was used in Sec. III. Generally, when the exponent in Eq. (7) takes values $\eta > 1$, the process is called superdiffusion and the trajectories of the particles have long displacements. The transport is characterized by normal diffusion if the variance grows linearly with time, i.e., if $\eta=1$. Subdiffusive transport occurs when the exponent η takes values less than 1. The embedding map shows all the three main classes of diffusion processes as illustrated in Fig. 6. Subdiffusive behavior in the embedding map can be further classified into two subclasses, viz., one associated with the trapping regions with nonstationary states and the other with the trapping regions with stationary states. We analyze the behavior of these classes in detail below.

The phase diagram of Fig. 1 separates out the distinct dynamical regimes in the α-γ space. Here, we find it useful to obtain a phase diagram which classifies the main diffusion regimes as a function of the parameters α-γ. The value of the exponent η can be used for such a classification. For this, the log-log plot of the variance as a function of time is fitted to

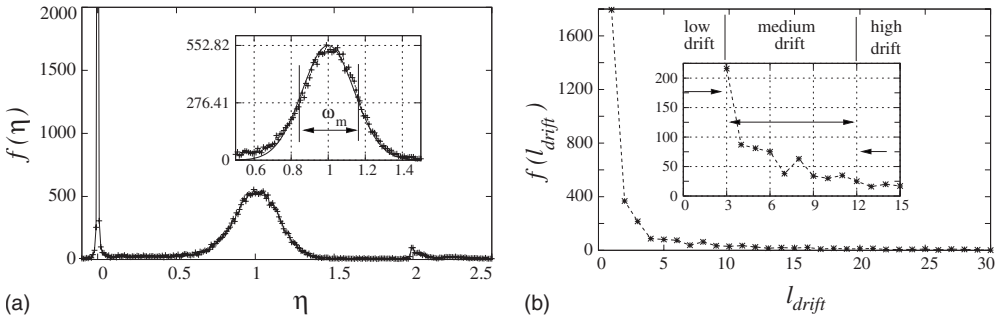

FIG. 7. The probability distribution of the exponents η in the phase diagram, showing three clear peaks. The inset shows the peak centered in $\eta=1$ for which the full width at half maximum ω_m is in the range $0.835 < \eta < 1.165$ that will delimit the normal diffusion exponents. The peak value at $\eta=0$ is $f(\eta)=6000$. (b) The probability distribution of drifts in the phase diagram has three classes, viz., high drifts ($\overline{l_{drift}} > 12$), medium drifts ($12 > \overline{l_{drift}} > 3$), and low drifts ($3 > \overline{l_{drift}}$) (see inset).

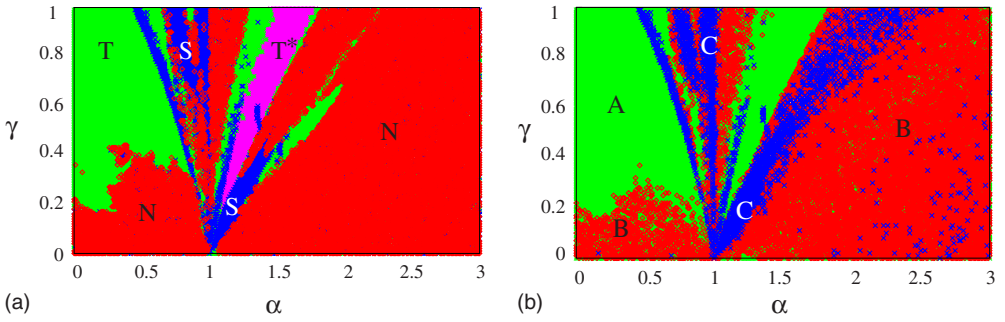

FIG. 8. (Color online) (a) The phase diagrams showing the four diffusion regions in the embedding map in the α-γ parameter space: superdiffusive regime is marked by S (blue), normal diffusive regimes are marked by N (red), subdiffusion with stationary states is marked by T* (pink), and subdiffusion with nonstationary states is marked by T (green). (b) The phase diagram shows the drifts of particles in the α-γ parameter space. The regions marked in "blue" have large average drifts, $l_{drift} > 12$ (labeled by "C"), regions in "red" have medium average drifts, $12 > l_{drift} > 3$ (labeled by "B"), and regions in "green" have low drifts, $l_{drift} < 3$ (labeled by "A"). This is for 3000 time steps averaged over 100 random initial conditions uniformly distributed in phase space.

a straight line after the initial transients. We used a linear square fit for finding the value of η for each data point in the α-γ parameter space.

Theoretically, the normal diffusion regions in the phase diagram can be distinguished from the anomalous diffusion regions if the values of the exponent $\eta > 1$ and $\eta < 1$. When dealing with numerical data, the normal diffusion regions cannot be identified by selecting the ones with the exponent $\eta = 1$. The distribution of the values of η in the entire phase diagram is shown in Fig. 7(a) and shows three peaks centered at $\eta \sim 0$, $\eta \sim 1$, and $\eta \sim 2$. The inset shows the distribution centered at $\eta \sim 1$ that can be fitted with a Gaussian. The standard deviation of the Gaussian is $\sigma_{Gauss} = 0.14$, and the full width at half maximum (ω_m) for this Gaussian, expressed as $\omega_m = 2\sigma_{Gauss}\sqrt{2\ \log(2)} = 2.3548\sigma_{Gauss}$, turns out to be 0.33 [see the inset of Fig. 7(a)]. This ω_m centered at $\eta = 1$ can therefore be taken as a good practical bound on the η to demarcate normal and anomalous diffusion regimes. The upper and lower bounds on the normal diffusion region are $\eta_{lower} = 1 - \omega_m/2$ and $\eta_{upper} = 1 + \omega_m/2$, respectively. The exponent values that demarcate the regions of the normal diffusion are therefore $\eta_{normal} \in [\eta_{lower}, \eta_{upper}]$. The cases which have values less than the lower bound η_{lower} are identified as subdiffusive and the ones which have values higher than the upper bound η_{upper} are identified as superdiffusive.

We note that in generating the phase diagram for diffusion regimes we have used 3000 time steps with 100 initial conditions distributed uniformly randomly in the phase space. For the phase diagrams in Fig. 8 a resolution of 0.01 in both the directions was used.

The diffusive phase diagram indicates the following transport properties. The phase diagram shown in Fig. 8(a) has normal diffusion regions in the regions that are labeled "N" (colored red), which are predominantly seen in the areas where the mixing is seen in the phase space (see Fig. 1). The superdiffusive regions labeled "S" (colored blue), as mentioned above, are identified where $\eta > 1.165$. On comparing these regions with the phase diagram of the dynamical regimes, it is clear that the superdiffusive regions coincide largely with the periodic regime.

The subdiffusive region is delimited by the criterion $\eta < 0.835$. It is easy to see that these regions mostly coincide with the chaotic structure regimes seen in Fig. 1. Further, there are two types of subdiffusion occurring here, viz., those associated with trapping in stationary states and trapping in nonstationary states. On the aerosol side of the phase diagram (colored green and labeled "T"), particles behave as though they are trapped in an attractor, but their dispersion grows sublinearly with time [Fig. 6(c)]. The cover phase space for such a typical case is seen in Fig. 9(a). On the other hand, in the bubble region (colored pink and labeled "T*"), particle trajectories get trapped forever and become stationary. Figure 9(b) shows the cover phase space for, the case, trapping into stationary states. As a result of the motion tending to fixed points, the variance tends to a constant value without any fluctuation after the transient time as seen in Fig. 6(d).

There are certain parameter regimes at which the particles do not diffuse beyond a given region in the phase space and

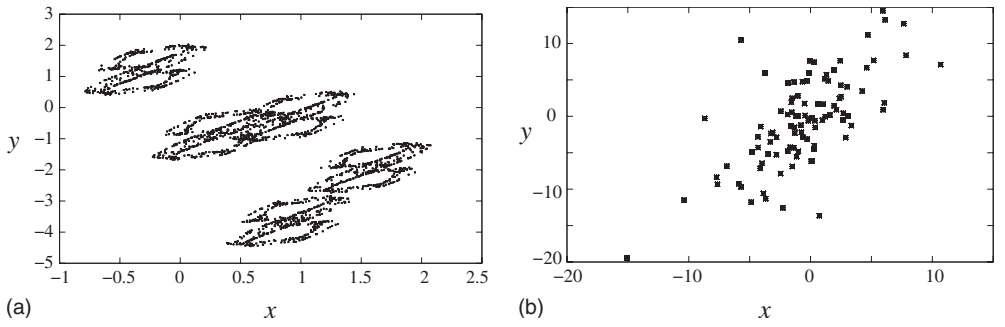

FIG. 9. The phase space plots of the subdiffusion regimes: (a) nonstationary states and (b) trapping states with stationary points.

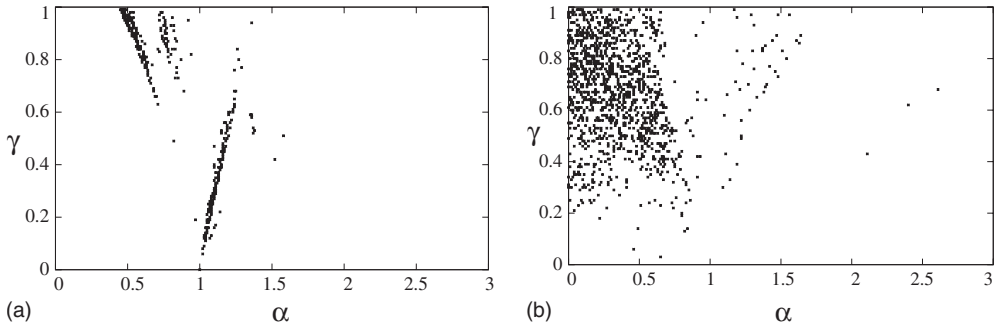

FIG. 10. (a) The phase diagram shows the regions characterized by ballistic diffusion. Here the diffusion exponent takes values $\eta=2$. (b) The phase diagram with points marked showing regions where the average drift $l_{drift}\sim 0$.

we saw that they belong to the subdiffusive regions. The average drift of the particles can be used to quantify the overall drift of the particle cloud from the initial position it started with. The drift is defined as the mean position of the cloud of the particles after a time t, i.e., $l_{drift}=\bar{l}(t)-\bar{l}(0)$, i.e., where l_{drift} is the difference between the average position $\bar{l}(t)$ of the cloud of the particles in cover space at time t from that at the time $t=0$. The distribution of the average drifts of the particle cloud for the range of values of α-γ discussed in the phase diagram is plotted in Fig. 7(b). It is clear from Fig. 7(b) that there are three main ranges of drifts. The large drifts are identified by the criterion $l_{drift}>12$, the intermediate ranges of drift by $3<l_{drift}<12$, while the small drifts are identified to have drift rates $l_{drift}<3$ [see inset of Fig. 7(b)].

A phase diagram for the drifts in the α-γ space is plotted in Fig. 8(b). Regions of large drift are colored blue, those of intermediate drift are colored red, and green regions have small drift. In comparing the parameter regions T^* (pink) in Fig. 8(a) where particles are trapped and become stationary, with the corresponding region of Fig. 8(b), it is clear that the particles here have low values of drift. The regions of high drifts in Fig. 8(b) overlap with the superdiffusion regions S (blue) both in the aerosol and the bubble regimes in Fig. 8(a). Therefore, there is good correlation between the phase diagrams constructed from the dispersion and drift criteria.

The phase diagrams obtained in Fig. 8 show no clear contiguous areas defining the three diffusion regimes or the three drift regimes, and these regions are seen to be interspersed in some areas of the phase diagrams. This is due to the fact that the values of the slope η and the average drift l_{drift} belong to continuous distributions which are partitioned into three regions. Hence sharp demarcations are not achieved.

We note that the embedding map also shows a region corresponding to the ballistic superdiffusion regime [21] which is characterized by a diffusion exponent $\eta\sim 2$ and has been earlier seen in diverse contexts such as the motion of atoms, molecules and clusters on solid surfaces [37], and in random walk models with random velocities [38]. This regime is shown in the phase diagram [Fig. 10(a)]. We note that this regime is seen at the edges of the periodic tongues. It is also useful to have a phase diagram to locate the regions where the average drift is zero, $l_{drift}\sim 0$. Figure 10(b) shows the regions of near zero drift and in reference to Fig. 8(b), we can see that it forms a subset of the regimes of the slowest drifts, marked in green (labeled "A").

It is important to note that characterization and classification of different diffusion and drift regimes are very useful in real application contexts. We expand on this point in Sec. VIII.

V. BEHAVIOR OF THE INITIAL TRANSIENT

The phase diagrams of Sec. IV have been obtained after the systems have equilibrated after an initial transient. However, the behavior of the initial transient can itself be quite different in the case of distinct dynamical regimes. We illustrate this for the dynamical regimes of the embedding map.

We examine the probability distribution of the jump lengths, i.e., the Euclidean distance between successive iterates, for transient times up to 500 iterates in regimes corresponding to periodic, chaotic, and mixing behavior. Here, 1000 initial conditions are spread uniformly randomly in the phase space for this analysis. Figure 11(a) shows the probability distributions of the jump lengths of the trajectories in the regime $(\alpha=0.5,\gamma=0.5)$, where chaotic structures are seen in the phase space. The distribution is clearly characterized by a heavy tail. Similar heavy tails characterize the jump length distribution of the trajectories seen at other points in the chaotic structure regime. In the region of the heavy tail the envelope can be fitted by the function

$$f_{Levy}(l)=\kappa\sqrt{\frac{\nu}{2\pi}}\frac{1}{(l-\delta_l)^{3/2}}\exp\left(\frac{-\nu}{2(l-\delta_l)}\right), \qquad (8)$$

where the parameters take the values $\nu=0.42$ and $\delta_l=0.34$ and the scale factor is $\kappa=11$ for the case shown in Fig. 11(a). On the other hand, the envelope of the distribution of jump lengths of trajectories for parameter values in the mixing regime $\alpha=2.8$, $\gamma=0.1$ shows Gaussian behavior. In Fig. 11(b) the envelope of the distribution has been fitted with a Gaussian function, $f_{Gauss}(l)=\frac{1}{\sigma\sqrt{2\pi}}\exp(-\frac{(x-\mu)^2}{2\sigma^2})$, with $\mu=0.95$, $\sigma=0.58$.

Thus, in the initial transient in the chaotic structure regime, the distribution of jump lengths peaks at short values but decays with a power-law tail, characteristic of the sticky regions. On the other hand, the jump length distribution in the mixing regime shows normal behavior, indicating rapid mixing of the initial conditions.

The cumulated jump distributions show this very clearly. The cumulated jump length distributions in the chaotic struc-

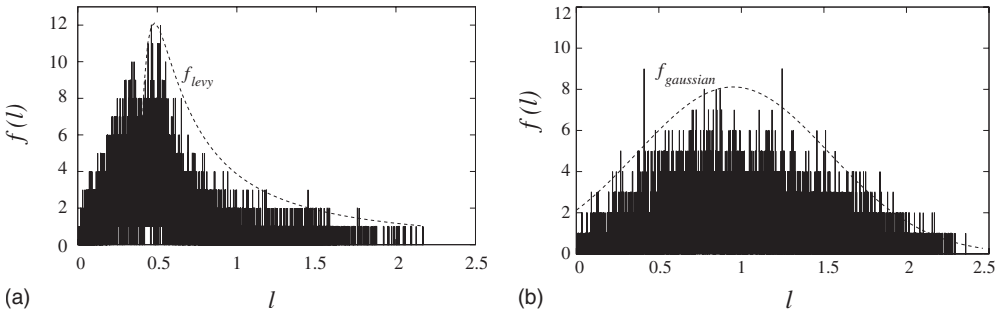

FIG. 11. The envelope of the distribution of flight lengths of trajectories in the periodic and chaotic structure regimes is fitted with a heavy tailed distribution. (a) The periodic regime (α=0.5, γ=0.5). (b) In the mixing regime the envelope is fitted by a Gaussian (α =2.8, γ=0.1). In both the plots 8000 bins were used for averaging in the x axis.

ture regime show power-law behavior [see Fig. 12(a)], whereas the distributions in the mixing regime conform to a cumulated Gaussian [see Fig. 12(b)]. The same function $f_{Gauss}(l)$ given above is used to obtain the cumulated distribution $F(l)$.

VI. TRANSPORT IN THE UDV REGION

It was reported recently that the embedding map system studied here experiences a severe form of nonhyperbolicity in the aerosol regime in the neighborhood of the parameter values α=0.8, γ=0.40 [39]. A crisis is seen in the system at these parameter values. The nonhyperbolicity in higher dimensional systems, in general, manifests itself as UDV with an accompanying breakdown of the shadowing theorem. The signatures of the presence of unstable dimension variability in the embedding map were seen in the fluctuation of the Lyapunov exponent around zero (see Fig. 13). The presence of UDV was confirmed from the distribution of the finite time Lyapunov exponents which showed that the spectrum is equally distributed in both positive and negative exponents [39].

The UDV region is found at an interface between two dynamical regimes, for example, in the above case, it is in seen at the interface between the periodic and the chaotic structure regimes. The transport properties of the system are studied in this region. However, due to the breakdown of shadowing at long times, computations are carried out for short times. Since the region where the UDV is seen lies between the periodic and chaotic structure regimes, the statistical properties such as the recurrence time statistics and the diffusion properties will have contributions from both the periodic and the chaotic structure regimes.

The cumulative recurrence time statistics for a typical point in the UDV regime is shown in Fig. 14(a). There is an exponential decay of recurrence times at intermediate time scales, as seen for the recurrence time distribution in the chaotic structure regime. The periodic regime has its signature at the short and long time scales with the periodic behavior showing up as discrete steps in the plot. The plot of the variance of the particle cloud as a function of time for the same parameters is seen in Fig. 14(b). This is clearly a subdiffusive case with the slope $\eta \sim 0.6$, indicating the influence of the chaotic structures.

VII. CONNECTION BETWEEN THE DYNAMICAL AND TRANSPORT PROPERTIES

It is clear from the previous discussion that there is an intimate connection between the dynamical and statistical properties of the system. We summarize our inferences in this section.

The phase diagram of the dynamical regimes of the embedding map, a paradigm for the dynamics of inertial particles in fluid flows, contains three distinct dynamical regimes, viz., periodic orbits, chaotic structure regimes, and mixing behavior. There is also a clear distinction between the dynamical behavior in the aerosol regime and the dynamical

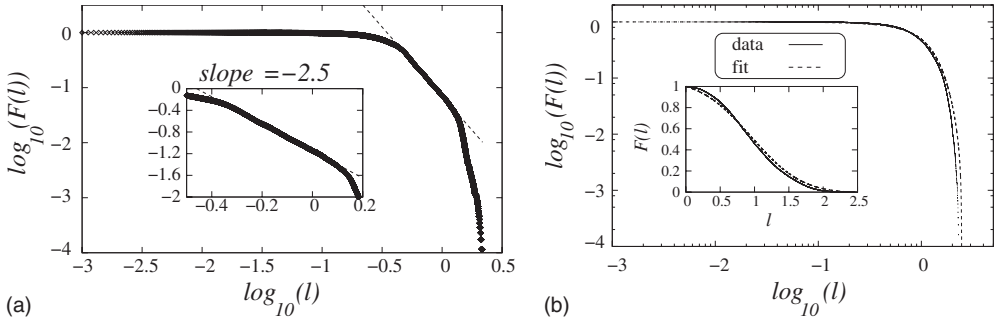

FIG. 12. The log-log plots of the cumulative probability distributions of the normalized jump lengths in (a) a typical trapping region (α=0.5, γ=0.5) showing a power-law tail with slope −2.5 and (b) a typical normal diffusion region (α=2.8, γ=0.1) showing the fit with a cumulative Gaussian distribution. In both the figures, 8000 bins were used for averaging.

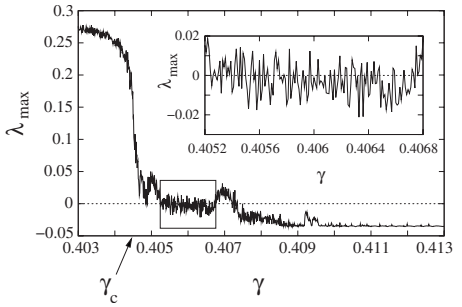

FIG. 13. The plot of λ_{max} vs γ showing sudden jump at crisis. The inset shows the fluctuation of λ_{max} around zero which is a signature of presence of UDV (fixed $\alpha=0.8$).

behavior in the bubble regime. Similar distinctions are seen in the recurrence time distributions and the diffusive and drift phase diagrams of the system.

The recurrence time statistics are useful in the regimes where no regular periodic behavior is seen, i.e., in the regions where the largest Lyapunov exponent is greater than zero. For the embedding map, these are the chaotic structure regime and the mixing regime. The cumulative recurrence time distribution for the chaotic structure regime shows an exponential decay followed by a power-law tail. The exponential behavior at short times reflects the mixing background in the inhomogeneous phase space. The power law seen here is the hallmark of the sticky regions in the phase space. The diffusion studies reveal that the chaotic structure regime shows subdiffusive character on the average. The distribution of jump lengths in the transient regime has an envelope that conforms to a Levy distribution, indicating that while short jumps dominate the distribution, the number of long jumps is sufficiently large to contribute a power-law tail.

The mixing regime, as expected, shows the exponential decay of the recurrence time distribution. The transport in this regime shows normal or Brownian diffusion, where the variance grows linearly with time. Normal diffusive behavior is predominant in the mixing regime on both the aerosol and bubble sides. The distribution of jump lengths in this regime has a Gaussian envelope.

Two phase diagrams, viz., the diffusion and the drift phase diagrams, were constructed in the α-γ parameter space to compare the nature of diffusion and dynamics in all the dynamical regimes of the embedding map. It was found that three main types of diffusion, viz., normal (Brownian type), subdiffusive, and superdiffusive types, are seen in the system. As mentioned above, normal diffusion is the dominant behavior in the mixing regime on both sides of the phase diagram. Superdiffusive regions are seen in the periodic regime of the aerosols and in a part of the periodic regime of the bubbles. However, the periodic regime on the bubble side also contains a regime where the inertial particles are trapped and have zero drift. This regime has subdiffusive transport with stationary states. Here the variance saturates to a constant value after an initial sublinear rise. This regime shows behavior consistent with early studies of impurity behavior [40], where it was observed that bubbles were pushed toward the islands forming regions of preferential concentration.

Subdiffusive transport is also seen in the chaotic structure regime on the aerosol side of the phase diagram where trapped states are also seen. However, the trapped states are nonstationary over here. Here, the variance fluctuates about a constant value after the initial sublinear rise. On the other hand, normal diffusion is predominant in the chaotic structure regime on the bubble side of the phase diagram. Ballistic diffusion similar to that seen in many natural processes is also seen in the embedding map. The regions of ballistic diffusion in the embedding map lie on the boundaries of the periodic regimes. The embedding map also shows the existence of unstable dimension variability at the boundary between the periodic regime and the chaotic structure regime. Thus, the signatures of both the regimes are seen in the recurrence time distribution. However, the transport behavior is clearly subdiffusive.

VIII. CONCLUSIONS

The transport properties of bailout embedding map, a paradigm to model the dynamics of inertial particles, are studied in this paper. The base fluid flow is assumed to be incompressible and modeled by an area-preserving map, the standard map. The resulting embedding map is dissipative and captures the qualitative dynamics of both particles that are heavier than the fluid, the aerosols, and lighter than the fluid, the bubbles. The main dynamical regimes in the embedding map system are reviewed and the statistical characterizers of transport in each distinct dynamical regime are

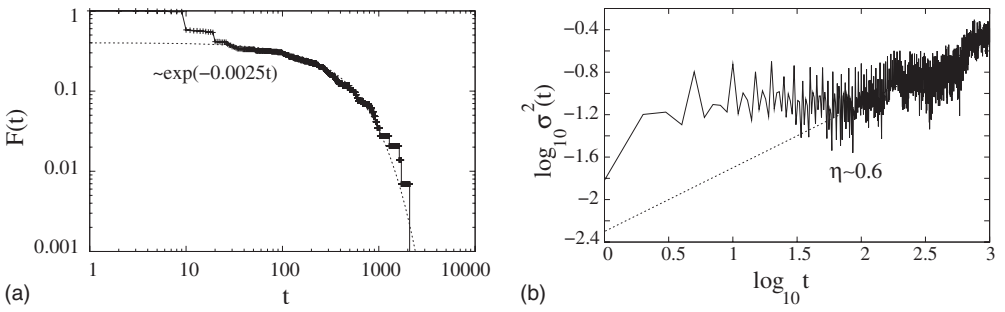

FIG. 14. (a) The cumulative recurrence time distribution showing an exponential fall in the intermediate time range. The discrete plateaus like behavior in the small and large time scales are due to the periodic nature. (b) The variance as a function of time in the UDV case shows subdiffusive behavior. The parameter values are $\alpha=0.8$, $\gamma=0.4062$.

evaluated. These are the recurrence time statistics and the diffusion and drift properties of system. An intimate connection is observed between the dynamical and statistical properties of the system.

The predominant dynamical regimes in the system are the periodic regime, the chaotic structure regime, and the mixing regime. These, together with the nature of the inertial particles, viz., whether aerosol or bubble, influence the diffusion, drift, and recurrence properties of the system. The mixing regimes of the system show normal diffusion and exponential decay of recurrence times indicating short term correlations in the system. Chaotic structure regimes possess inhomogeneous sticky regimes in the phase space, and these contribute power-law tails to the recurrence time distributions and jump length distributions. Superdiffusive behavior is seen in the periodic regimes of both aerosols and bubbles. However, some trapping regimes are seen in both the aerosol and bubble cases, and these show subdiffusive behavior and low drifts, including zero drifts in the case of stationary states.

Our results may have implications in the context of realistic applications. It was found that the average drift is close to zero in the trapping regions. This may have important consequences in practical contexts. For example, consider flows with reacting impurities. Chemical species that have low diffusion and low drift rates can get localized and concentrated in certain regions. These can then react with other chemical species and cause their enhancement or depletion, with further consequences for the environment.

Rapid transport, as in the case of superdiffusive case, can provide a mechanism by which impurities can easily access wider regions in the available space. This maybe desirable or undesirable, depending on the context. For example, smoke emanating from a chimney containing particulate matter with fast diffusion and slow drift can spread the pollutants in the proximity of the source rather than carrying it off to farther places. On the other hand, this regime may be highly useful in the context of nutrients spreading through a fluid.

The phase diagrams of the system indicate that a rich variety of dynamical and statistical regimes is available to inertial particles in fluids. Specific choices of regime may be suitable for a specific application. Hence the insights gained from these diagrams may be useful in varied application contexts.

ACKNOWLEDGMENTS

N.N.T. thanks CSIR, India for financial support and N.G. thanks DST, India for partial financial support under Project No. SP/S2/HEP/10/2003.

[1] R. E. Newell, V. Thouret, J. Y. N. Cho, P. Stoller, A. Marenco, and H. G. Smit, Nature (London) **398**, 316 (1999).
[2] P. H. Haynes, in *Transport, Stirring and Mixing in the Atmosphere: Mixing, Chaos and Turbulence*, edited by H. Chate, E. Villermaux, and J. M. Chomaz (Kluwer, Dordretch, 1999).
[3] R. T. Pierrehumbert, Phys. Fluids A **3**, 1250 (1991).
[4] H. Aref, J. Fluid Mech. **143**, 1 (1984).
[5] J. M. Ottino, *The Kinematics of Mixing: Stretching, Chaos and Transport* (Cambridge University Press, Cambridge, 1989); R. Sturman, J. M. Ottino, and S. Wiggins, *The Mathematical Foundations of Mixing* (Cambridge University Press, Cambridge, 2006).
[6] L. Kuznetsov and G. M. Zaslavsky, Phys. Rev. E **61**, 3777 (2000).
[7] I. J. Benczik, Z. Toroczkai, and T. Tel, Phys. Rev. E **67**, 036303 (2003).
[8] R. D. Vilela, T. Tel, A. P. S. de Moura, and C. Grebogi, Phys. Rev. E **75**, 065203(R) (2007).
[9] T. Nishikawa, Z. Toroczkai, C. Grebogi, and T. Tel, Phys. Rev. E **65**, 026216 (2002).
[10] R. Reigada, F. Sagues, and J. M. Sancho, Phys. Rev. E **64**, 026307 (2001).
[11] A. E. Motter, Y. C. Lai, and C. Grebogi, Phys. Rev. E **68**, 056307 (2003).
[12] N. N. Thyagu and N. Gupte, Phys. Rev. E **76**, 046218 (2007).
[13] J. H. E. Cartwright, M. O. Magnasco, and O. Piro, Phys. Rev. E **65**, 045203(R) (2002).
[14] M. R. Maxey, Phys. Fluids **30**, 1915 (1987).
[15] R. T. Pierrehumbert, Chaos **10**, 61 (2000); D. R. Fereday, P. H. Haynes, A. Wonhas, and J. C. Vassilicos, Phys. Rev. E **65**, 035301(R) (2002).
[16] E. G. Altmann, A. E. Motter, and H. Kantz, Phys. Rev. E **73**, 026207 (2006).
[17] M. R. Maxey and J. J. Riley, Phys. Fluids **26**, 883 (1983).
[18] A. Babiano, J. H. E. Cartwright, O. Piro, and A. Provenzale, Phys. Rev. Lett. **84**, 5764 (2000).
[19] N. Gupte and N. Nirmal Thyagu, in *Nonlinear Dynamics (Proceedings of the Conference Recent Developments Nonlinear Dynamics)*, edited by M. Daniel and S. Rajasekar (Narosa, New Delhi, 2009).
[20] G. M. Zaslavsky and M. K. Tippett, Phys. Rev. Lett. **67**, 3251 (1991).
[21] G. M. Zaslavsky, Phys. Rep. **371**, 461 (2002).
[22] B. V. Chirikov, Phys. Rep. **52**, 263 (1979).
[23] R. B. White, S. Benkada, S. Kassibrakis, and G. M. Zaslavsky, Chaos **8**, 757 (1998).
[24] In the context of the bailout embedding equation [Eq. (1)], the regime $\alpha>3$ is unphysical as it implies negative particle densities. While the $\alpha>3$ regime cannot be deemed unphysical by such a direct physical argument in the context of the bailout standard map, the regimes beyond $\alpha>3$ turn out to be mixing regimes for all values of γ and hence have not been plotted in the phase diagram.
[25] J. B. Gao, Phys. Rev. Lett. **83**, 3178 (1999).
[26] V. Balakrishnan, G. Nicolis, and C. Nicolis, J. Stat. Phys. **86**, 191 (1997).
[27] V. Balakrishnan, G. Nicolis, and C. Nicolis, Phys. Rev. E **61**, 2490 (2000).
[28] E. G. Altmann and H. Kantz, Phys. Rev. E **71**, 056106 (2005).
[29] B. V. Chirikov and D. L. Shepelyansky, Phys. Rev. Lett. **82**,

528 (1999).
[30] R. Artuso, L. Cavallasca, and G. Cristadoro, Phys. Rev. E **77**, 046206 (2008).
[31] N. Buric, A. Rampioni, G. Turchetti, and S. Vaienti, J. Phys. A **36**, L209 (2003).
[32] The effect of the finite size of the intervals in prototypical systems such as the logistic map and the Henon map is well understood [41].
[33] E. Ott, *Chaos in Dynamical Systems* (Cambridge University Press, Cambridge, 2002).
[34] The dynamic origin of the chaotic structures lies in an attractor widening crisis. The details of this crisis are discussed in [12].
[35] T. H. Solomon, Eric R. Weeks, and Harry L. Swinney, Physica D **76**, 70 (1994).
[36] For values of the parameters α and γ that show a power-law decay at asymptotic times, the exponent is always found to be $\zeta < -2$. This is in conformity with Kac's lemma that for the distribution to have finite moments the absolute value of the exponent should be greater than 2 [21,42].
[37] A. M. Lacasta, J. M. Sancho, A. H. Romero, I. M. Sokolov, and K. Lindenberg, Phys. Rev. E **70**, 051104 (2004).
[38] V. Zaburdaev, M. Schmiedeberg and H. Stark, Phys. Rev. E **78**, 011119 (2008).
[39] N. N. Thyagu and N. Gupte, Pramana **70**, 1031 (2008).
[40] J. Eaton and J. Fessler, Int. J. Multiph. Flow **20**, 169 (1994).
[41] E. G. Altmann, E. C. da Silva, and I. L. Caldas, Chaos **14**, 975 (2004).
[42] G. M. Zaslavsky, *The Physics of Hamiltonian Systems* (Imperial, London, 2007).